ISSN (Print) 1226-1750
ISSN (Online) 2233-6656
Journal of Magnetics 25(3), 415-427 (2020) https://doi.org/10.4283/JMAG.2020.25.3.415

Auto Segmentation Method for Electromagnetic Radiation Camera Myocardial Images

Seokyoon Choi and Jeongmin Seo*

Department of Radiological Science, Catholic University of Pusan, #57 Orynndaero, Geumjeonggu, Busan 46252, Republic of Korea

(Received 13 November 2019, Received in final form 25 September 2020, Accepted 25 September 2020)

Electromagnetic radiation camera (ERC) provides functional information about the left ventricle. We need new methods of quantitative analysis, such as the segmentation myocardial images for maximum utilization of ERC. The level set method(semi-automatic) based approach method that has excellent potential with regarding mapping topological change in 2D images but the crucial point is when stopping iteration to obtain the optimal segmentation result. This study suggests the Courant–Friedrichs–Lewy (CFL) condition, feature measurement index (FMI), and modified Thompson Tau technique (MTTT) to investigate the optimal convergence problem. The CFL condition contributes to the stable numerical iteration of the level set, whereas the FMI and MTTT are used for exact iteration stopping. This study compared the auto segmentation method and the manual segmentation method through assessments. The results were so matched (82.39±13.92 %) so we can develop a 3D model that could be used to diagnose ischemic heart disease and infarction. The proposed segmentation method can help to diagnose the disease conveniently and accurately in the clinic.

Keywords : myocardial image, image segmentation, ERC

1. Introduction

Electromagnetic radiation camera (ERC) is very useful in the quantitative analysis of metabolic images and evaluation of the hemodynamic importance of coronary artery disease, among other applications, and has helped to deliver cardiac diagnoses using a noninvasive method [1, 2], but researchers reported conflicting values for the sensitivity and specificity of ERC.

Our study aims to quantitatively support ERC myocardial imaging. Accurate image segmentation is necessary for quantitative calculation. In this study, we use a new segmentation method which ERC images exhibit a blurring phenomenon due to radiation scattering, collimator-detector, photon attenuation, and motion artifacts from patients's movement. This phenomenon can generate low resolution and high noise level in the ERC images which may cause misdiagnosis and errors in quantitative analysis.

Recently, various image segmentation methods have been studied to segment the myocardiac in ERC. Dornheim [6] successfully achieved auto segmentation using a mass spring model, but the result was neither accurate nor smooth. Yang [7] presented a new deformable model for object detection based on charged particle dynamics, while Tan [8] presented a segmentation model using an active shape model, but involved various constraints.

Meanwhile, solutions for ERC are currently being proposed to segment LV in ERC using the level set formulation. The point of level-set is the introduction of geometrical concentrate into the derivation of the Euler-Lagrange equation; the segmentation of each individual frame can be interpreted as the closed boundary of an object [9]. Kohlberger [10] presented a new thickness term for the epi- and endocardium using level set, and approximated the level set description using a compact PCA subspace representation.

The starting point is the CV (chan and vese) model [11]. This model uses a different way as compared to the traditional level set. This method can detect contours as objects with very smooth or discontinuous boundaries, but this method has complex operation processes and computational waste from numerical iteration processes.

The level set has a continuous spatial-temporal partial differential equation solution. The finite difference scheme and numerical approximation solution have been applied

©The Korean Magnetics Society. All rights reserved.
*Corresponding author: Tel: +82-51-510-0581
Fax: +82-51-510-0588, e-mail: prayersjm@gmail.com

© 2020 Journal of Magnetics

a level set–based applications [9-15]. However, the level set did not consider numerical stability or optimal convergence in many applications. To overcome this problem, Chaudhury developed a new auto stopping rule with a circumference length index [16]. However, that only using the length index and feature measurement index (FMI) makes some difficulties in detecting the morphological change in sequential myocardial images on ERC images.

In this research, we propose a solution of stability problem and numerical iteration stopping problem, using the CV model to accurately segment the myocardial in ERC images. In addition, we suggest a 3D model from ERC images.

2. Materials and Methods

We set three steps for the process of optimal segmentation (Fig. 1): First, settling the stability problem. Second, manually assigning a heuristic iteration count to obtain myocardial features. Third, calculating the iteration stop count automatically from the FMI and modified Thompson Tau technique (MTTT). 28 myocardial ERC images were used to find excellent FMI. The following methods were used to evaluate the suggested segmentation method. Manual segmentation was repeatedly carried out 14 times by two experts and reference was made by a mean shape model. Manual segmentation of 280 times was conducted with a total of 28 images. Next step, how an automatic segmentation method accord with reference was evaluated through the area overlap ratio (AOR) and the simplex criterion value(SCV). For the simulation, PC (Intel® Core 2Duo CPU @ 2.93Ghz, 1.96GB RAM) and software (MATLAB R2008b, Massachusetts, U.S.A.) were used.

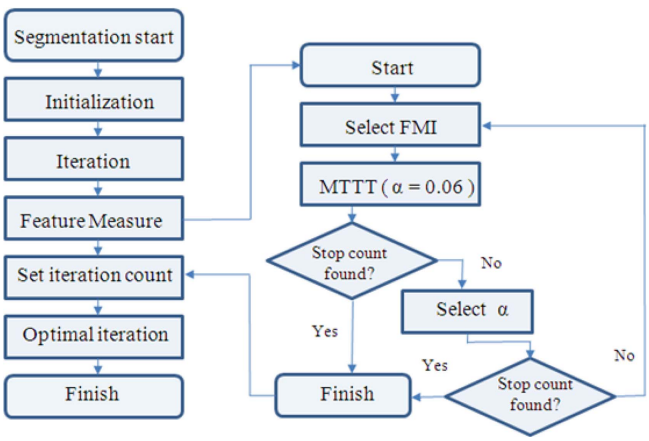

Fig. 1. (Color online) Diagram of the proposed segmentation process. Calculate excellent FMI, Delta, Alpha parameters then complete the optimal segmentation.

2.1. Basic Principles of ERC Imaging

A gamma-ray or gamma radiation is penetrating electromagnetic radiation arising from the radioactive decay of atomic nuclei. It consists of the shortest wavelength electromagnetic waves and so imparts the highest photon energy [34]. This imaging technique of nuclear medicine has several features in common with x-ray CT. Multiple views are obtained to compile an image of one or more axial image slices through the patient. The x-ray tube rotates and the detectors are stationary in 4th generation X-ray CT. Most transverse-section ERC systems employ a rotating detector and a stationary source of γ-rays [35, 36].

The detection of gamma rays are performed through using of a gamma camera, which consists of a scintillation crystal that optically coupled with an array of photomultiplier tubes (PMT), and this PMT converts gamma rays into electric signals.

2.2. Automatic Segmentation Algorithm

The classical segmentation method, such as thresholding, watershed, edge detection, and snake model was very sensitive to noise and exhibited obscured boundaries [22-25]. Therefore that post-processing of segmentation was required, but the CV model overcomes false segmentation from noise and irregular characteristics and identify topological change. So CV model assumes that curve C is on the 2D image that is divided into two regions and that the brightness value of the pixels is constant.

Curve C is represented by Eq. (1)

$$\begin{aligned} F(c_1, c_2, \phi) &= \mu \int_\Omega \delta(\phi(x,y))|\nabla\phi(x,y)|dxdy \\ &+ v\int_\Omega H(\phi(x,y))dxdy \\ &+ \lambda_1 \int_\Omega |u_0(x,y) - c_1|^2 H(\phi(x,y))dxdy \\ &+ \lambda_2 \int_\Omega |u_0(x,y) - c_2|^2 (1 - H\phi(x,y))dxdy \end{aligned} \quad (1)$$

μ: scale parameter. if $\mu = \infty$, then the length of the boundaries should be minimized
v, λ: nonnegative parameters
u_0: given image

Generally, the parameters are taken to be $v = 0$, $\lambda_1 = \lambda_2 = 1$

The solution is got by the next two steps, which are used to minimize energy.

Firstly, calculating C1 and C2 by Eq. (2); this calculation gives the minimum energy in relation to fixed ϕ:

$$c_1(\phi) = \frac{\int_\Omega u_0(x,y)H(\phi(x,y))dxdy}{\int_\Omega H(\phi(x,y))dxdy}$$

$$c_2(\phi) = \frac{\int_\Omega u_0(x,y)(1 - H(\phi(x,y)))dxdy}{\int_\Omega H(\phi(x,y))dxdy} \tag{2}$$

Secondly, obtaining the level set function with minimized energy from C1 and C2.

The energy-minimizing solution has to satisfy the Euler-Lagrange equation; the solution of the level set is obtained by Eq. (3):

$$\frac{\partial \phi}{\partial t} = \delta(\phi)\left(\mu \nabla \cdot \frac{\nabla \phi}{|\nabla \phi|} - v - \lambda_1 (u_0 - c_1)^2 + (u_0 - c_2)^2\right) \tag{3}$$

A numerical approximation of the level set model is obtained by Eq. (4)

$$\frac{\phi_{i,j}^{n+1} + \phi_{i,j}^{n}}{\Delta t} = \left(\delta_h(\phi_{i,j}^n)\left[\frac{\mu}{h^2}\Delta_-^x \cdot \left(\frac{\Delta_+^x \phi_{i,j}^{n+1}}{\sqrt{\frac{(\Delta_+^x \phi_{i,j}^n)^2}{(h^2)} + \frac{(\phi_{i,j+1}^n \ \phi_{i,j-1}^n)^2}{(2h)^2}}}\right) + \frac{\mu}{h^2}\Delta_-^x \cdot \left(\frac{\Delta_+^x \phi_{i,j}^{n+1}}{\sqrt{\frac{(\phi_{j+1,j}^n - \phi_{i-1,j}^n)^2}{(2h)^2} + \frac{(\Delta_+^x \phi_{i,j}^n)^2}{(h^2)}}}\right) - v - \lambda_1 (u_{0,i,j} - c_1(\phi^n))^2 + \lambda_1 (u_{0,i,j} - c_2(\phi^n))^2\right] \tag{4}$$

The algorithm solves as follows the Partial differential equation (PDE) in ϕ from Eq. (3) to obtain ϕ^{n+1} to discretize the equation in ϕ use a finite-differences implicit scheme. The algorithm is as follow; knowing ϕ^n the first compute $c_1(\phi^n)$ and $c_2(\phi^n)$. Second compute ϕ^{n+1} by the following discretization. This linear system is solved by an iterative method [11]. The segmentation result of images by iterative calculation and the evolution of the subjective surface are shown in Fig. 2. It has found that the results of segmentation are different by the iteration count. Figure 4(a) shows the final segmented area in test case B, represented by a binary image in Fig.

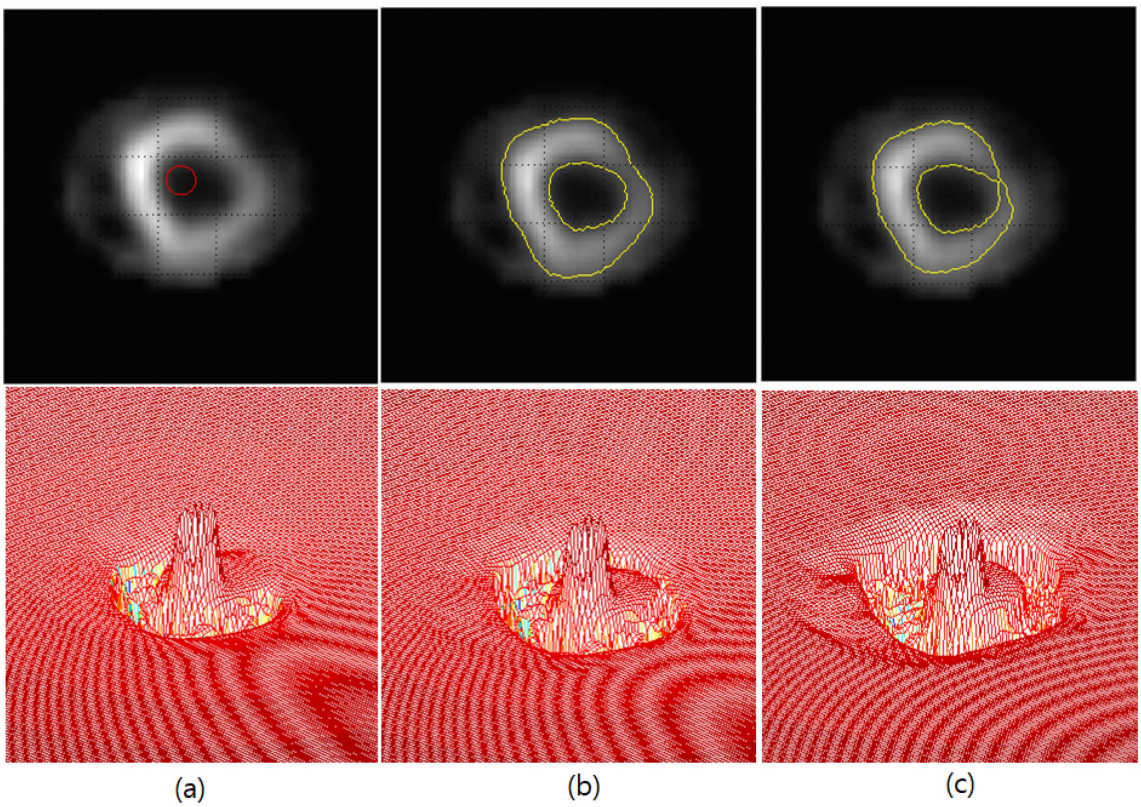

Fig. 2. (Color online) The results of segmentation for iteration of proposed method using MPS image sample. top: Final segmented area with proposed segmentation algorithm. Bottom: the evolution of the subjective surface. (a) iteration 5, (b) iteration 10, (c) iteration 80.

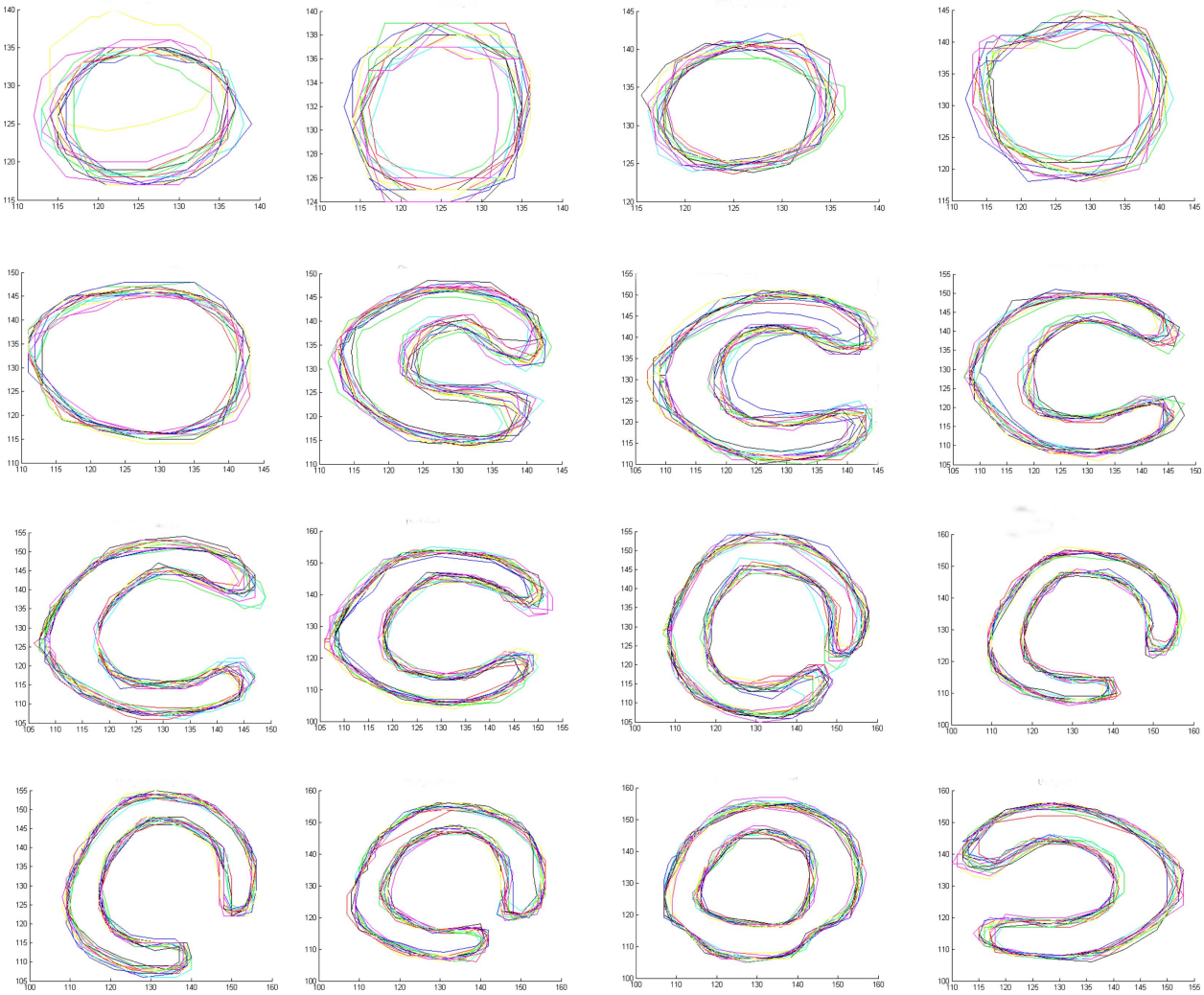

Fig. 3. (Color online) The results of training set to make mean shape (Test images).

4(b).

2.3. Stability and Auto stopping rule for Variational level set

2.3.1. Stability Using CFL Condition

While solving a numerical difference, some approximation error should occur. As time passes, unstable calculation process arise and the results will be inaccurate [12-13].

When we use a small Δt value In Eq. (3) and Eq. (5), the result is generally satisfactory but this has slow curve evolution. The large Δt value has a fast curve evolution, but the result is generally unsatisfactory.

$$\frac{\partial \phi}{\partial t} = \frac{\phi^{n+1} - \phi^{n}}{\Delta t} \tag{5}$$

We cannot know how big a value of Δt will be used. In [17, 18], $\Delta t = 0.0001$ was used, and Chan [11] used $\Delta t = 0.1$ for his approximation. Therefore, it is important to calculate optimal state in input images and to apply it to curve evolution.

$$F_{\max} \cdot \Delta t \le (h_x, h_y) \tag{6}$$

In this study, we used a Courant–Friedrichs–Lewy (CFL) condition [Eq. 6] to solve level set approximation and overcome the stability problem. h_x, h_y is the grid space of x-axis and y-axis. In Eq. (6), $F_{\max}$ is the absolute value of max velocity in all points on the Cartesian grid.

2.3.2. Feature Measurement Index (FMI)

It is so important to stop the curve evolution when exactly at the optimal convergence, which has a variational segmentation shape in each iteration process.

Moreover, feature-sensing technology is needed to detect changes in the myocardial from segmentation, so

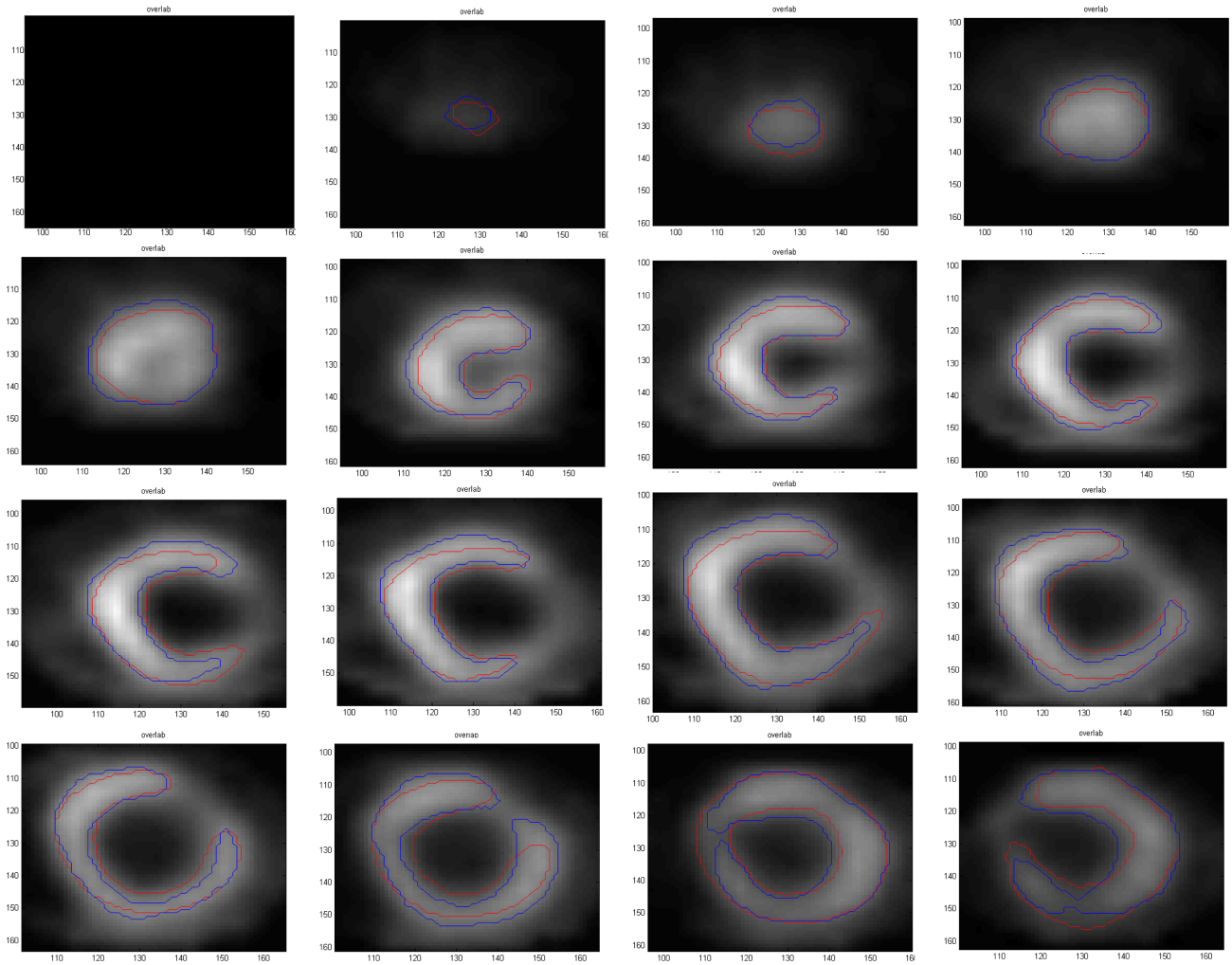

(a)

Fig. 4. (Color online) Result of reference and proposed auto segmentation of ERC images: (a) simultaneously displayed reference segmentation result (red line) and proposed auto segmentation result (blue line), (b) final proposed auto segmented area using binary image.

this research used feature measurement in the spatial domain. The feature measurements in this study include Eccentricity, FilledArea, ConvexArea, Solidity, and Extent. Thus, we defined five measurements in the FMI: EI, FaI, CaI, SI, and ExI. We use the regionprops function, from the image processing toolbox (MATLAB R2008b, Massachusetts, U.S.A.), to feature measurement that can identify properties used to stop the curve evolution [37].

An ellipse is the set of all points in a plane such that the sum of the distances from any point T to two fixed points F1 and F2 is a given constant, K. F1 and F2 are both foci of the ellipse (Fig. 5).

EI = foci/ major axis length
TF1 + TF2 = K

ConvexArea is the number of pixels in "ConvexImage.". The extent is the specified the ratio of pixels in the foreground region with the pixels in the total bounding box (Fig. 5).

2.3.3. Modified Thompson Tau Technique (MTTT)

The result of FMI data flow to stop level set iteration was got from the one of 2.2.2.

The MTTT is computed for each data point which values are compared to a reference. It was a tool developed by Rienzner [20, 21] to identify outliers, and can also be used to find the stopping point of an iteration to segment the myocardial myocardial region when using a level set algorithm.

Data was compared using the stopping indices of iteration. MTTT was used for verification of stopping points of the iteration. MTTT is based on the following

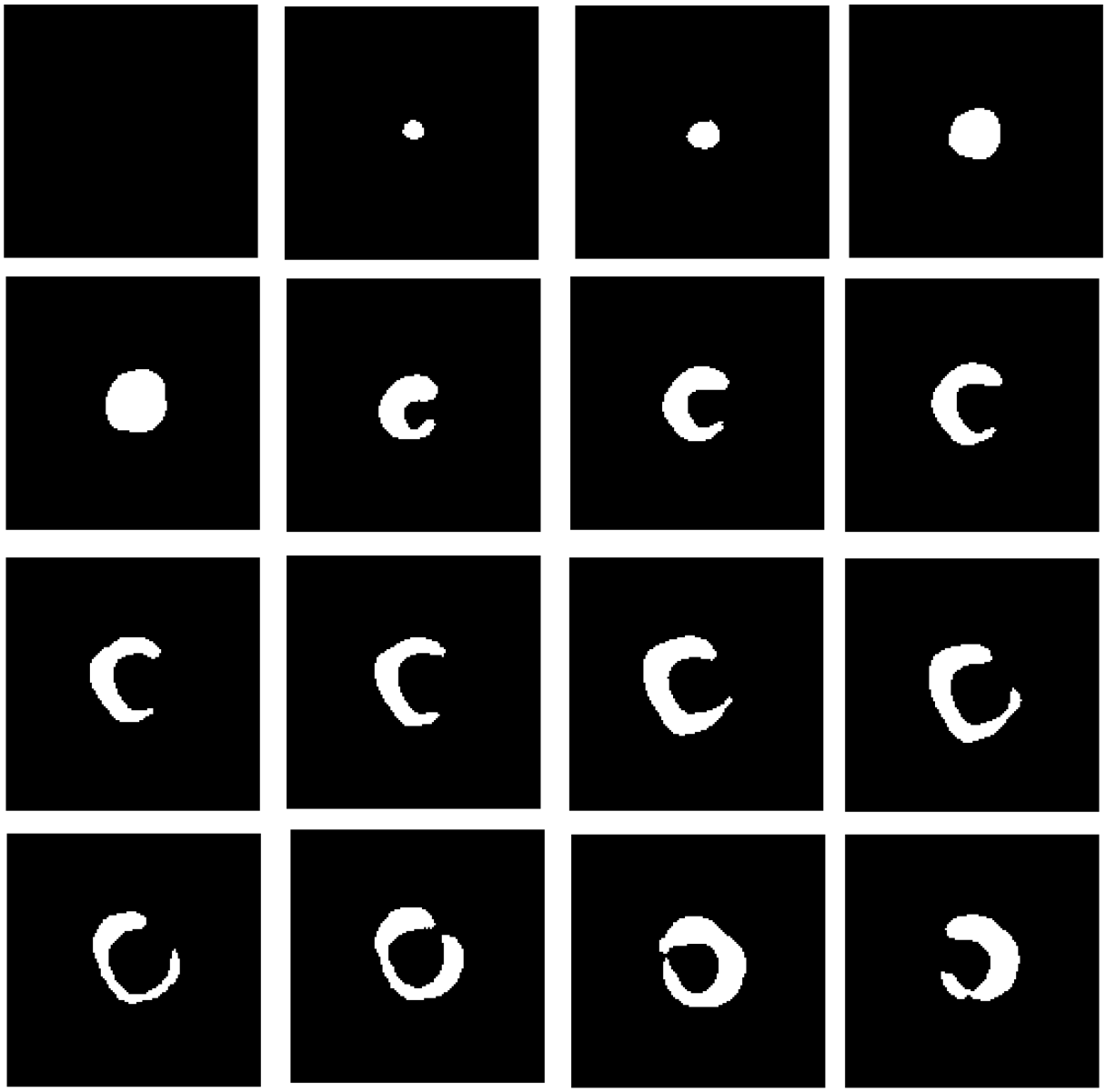

(b)

Fig. 4. Continued.

equation:

$$\delta_i = |x_i - x_{AVG}| > \tau SD \tag{7}$$

where x_i is the value to be tested, x_{AVG} is the average of all responses, SD is the standard deviation, and τ is the calculated value of the student's t PDF for a given data sample number n. If δ_i was greater than the Tau factor (τSD), the value was considered to be an outlier.

τ is calculated from the following equation:

$$\tau = \frac{t_{\alpha/2} \cdot (n-1)}{\sqrt{n}\sqrt{n-2+t_{\alpha/2}}} \tag{8}$$

where n is the number of data points, and $t_{\alpha/2}$ is the student's t value, based on $\alpha = 0.005$. If a data point is rejected as an outlier, MTTT removes it and starts over, calculating a new mean value and a new standard deviation and searching for more outliers.

2.4. Comparing of performance

Reference FMI was compared and evaluated with the mean shape model. For this, the differences between the segmentation result of the suggested algorithm and reference were shown using the AOR of Eq. (8) and they were compared with Eq. (9). The contents of the mean

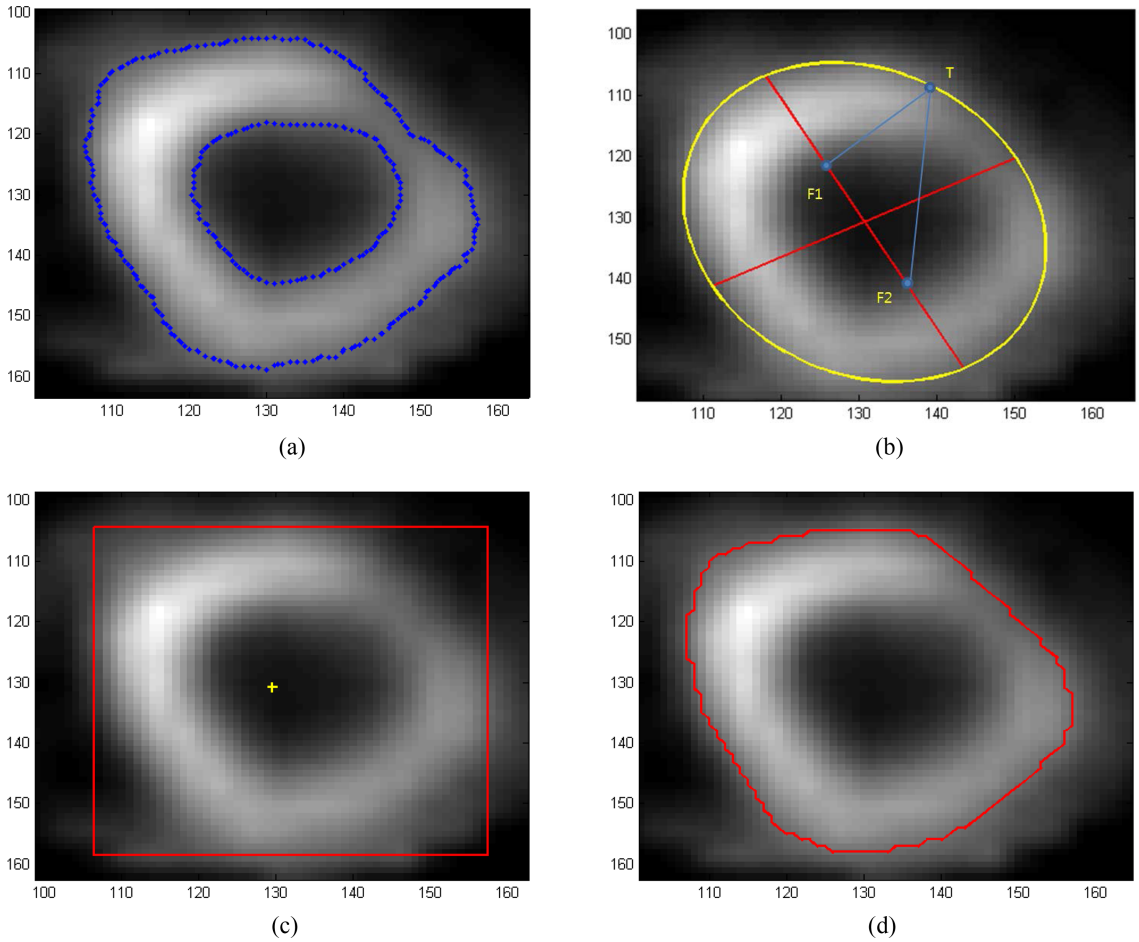

Fig. 5. (Color online) Feature measurement method in the spatial domain, features are selected automatically from the segmentation result: (a) final segmentation result, (b) the Eccentricity of an ellipse from segmentation result, (c) the minimum bounding rectangle from segmentation result, (d) the Convex hull from segmentation result.

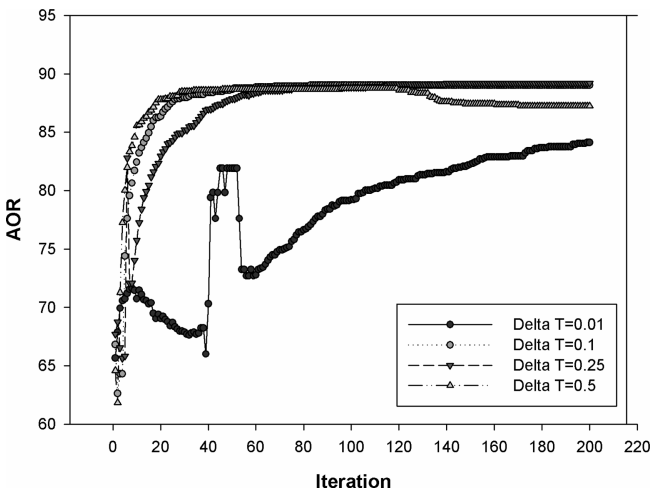

Fig. 6. The results of AOR value for iteration of proposed method.

shape model are as follows. Module 1, a process to assign landmarks in training sets to define the form of the study model. x_j, y_j coordinate sets are expressed by 2D vectors, and the numbers of landmarks and training sets can be applied diversely depending on the area of application. Module 2, a process to geometrically align collected landmarks, and not all the coordinates obtained from training sets are consistent. Module 3, the mean shape of local structure modeling will be calculated. The central point of each form in module 1 is calculated by Eq. (9). Through Eq. (10) and Eq. (11) in module 2, all matrixes are made to be of the same directions, same size and rotated around the central point to optimally align all study models. x_j, y_j coordinates sets in Eq. (9) represent the landmarks obtained from the edges of the study images. $(\bar{x}, \bar{y})$ was a set of the mean landmarks used to calculate the scales in Eq. (10). Therefore, the result will be the condensation of diversing sizes of contours for study into the same size. Eq. (11) represents a matrix transformation formula used to rotate the matrixes by angle θ around the origin point, and it serves to rotate all

coordinate sets for study in the same direction [29, 30].

$$(\bar{x}, \bar{y}) = \left(\frac{1}{n}\Sigma_{j=1}^{n}\ x_j,\ \frac{1}{n}\Sigma_{j=1}^{n}\ y_j\right) \tag{9}$$

$$S(x) = \sqrt{\Sigma_{j=1}^{n}[(x_j - \bar{x})^2 + (y_j - \bar{y})^2]} \tag{10}$$

$$T\begin{pmatrix} x \\ y \end{pmatrix} = \begin{bmatrix} a & -b \\ b & a \end{bmatrix}\begin{bmatrix} x \\ y \end{bmatrix} + \begin{bmatrix} t_x \\ t_y \end{bmatrix} \tag{11}$$

Table 1. Results show the auto stopping count and AOR for each FMI and Alpha value of MTTT (Use Δt = 0.25).

Alpha	Extent Index (EI)		Solidity Index (SI)		ConvexArea Index (CaI)		FilledArea Index (FaI)		Pixel count Index (PcI)	
	Count	AOR (%)	Count	AOR (%)	Count	AOR (%)	Count	AOR (%)	Count	AOR (%)
0.05	55.13 ± 55.83	84.35 ± 7.13	49.31 ± 57.51	82.39 ± 13.92	80.19 ± 66.35	84.39 ± 6.97	71.94 ± 64.34	82.95 ± 13.79	62.38 ± 60.54	82.49 ± 2.87
0.06	57.78 ± 55.14	84.31 ± 7.17	62.50 ± 67.62	82.41 ± 14.01	88.28 ± 67.83	84.35 ± 6.96	78.97 ± 65.20	82.92 ± 13.81	73.38 ± 66.62	83.63 ± 1.89
0.07	59.13 ± 55.30	84.31 ± 7.17	62.50 ± 67.62	82.41 ± 14.01	92.22 ± 67.75	82.84 ± 13.55	86.38 ± 66.85	82.80 ± 13.84	80.78 ± 68.86	80.72 ± 2.12
0.08	72.81 ± 64.02	84.24 ± 7.19	62.50 ± 67.62	82.41 ± 14.01	103.75 ± 65.99	82.90 ± 13.52	98.09 ± 70.60	82.74 ± 13.84	92.50 ± 73.44	80.74 ± 2.11
0.09	80.81 ± 65.40	84.19 ± 7.08	67.06 ± 71.87	82.52 ± 14.08	104.50 ± 66.98	82.70 ± 13.62	100.66 ± 72.84	82.72 ± 13.84	93.06 ± 72.79	80.73 ± 2.11
0.1	88.38 ± 63.73	84.16 ± 7.07	69.91 ± 71.79	82.56 ± 14.05	98.56 ± 66.69	82.72 ± 13.62	97.00 ± 73.23	82.75 ± 13.85	95.00 ± 71.55	80.78 ± 2.10

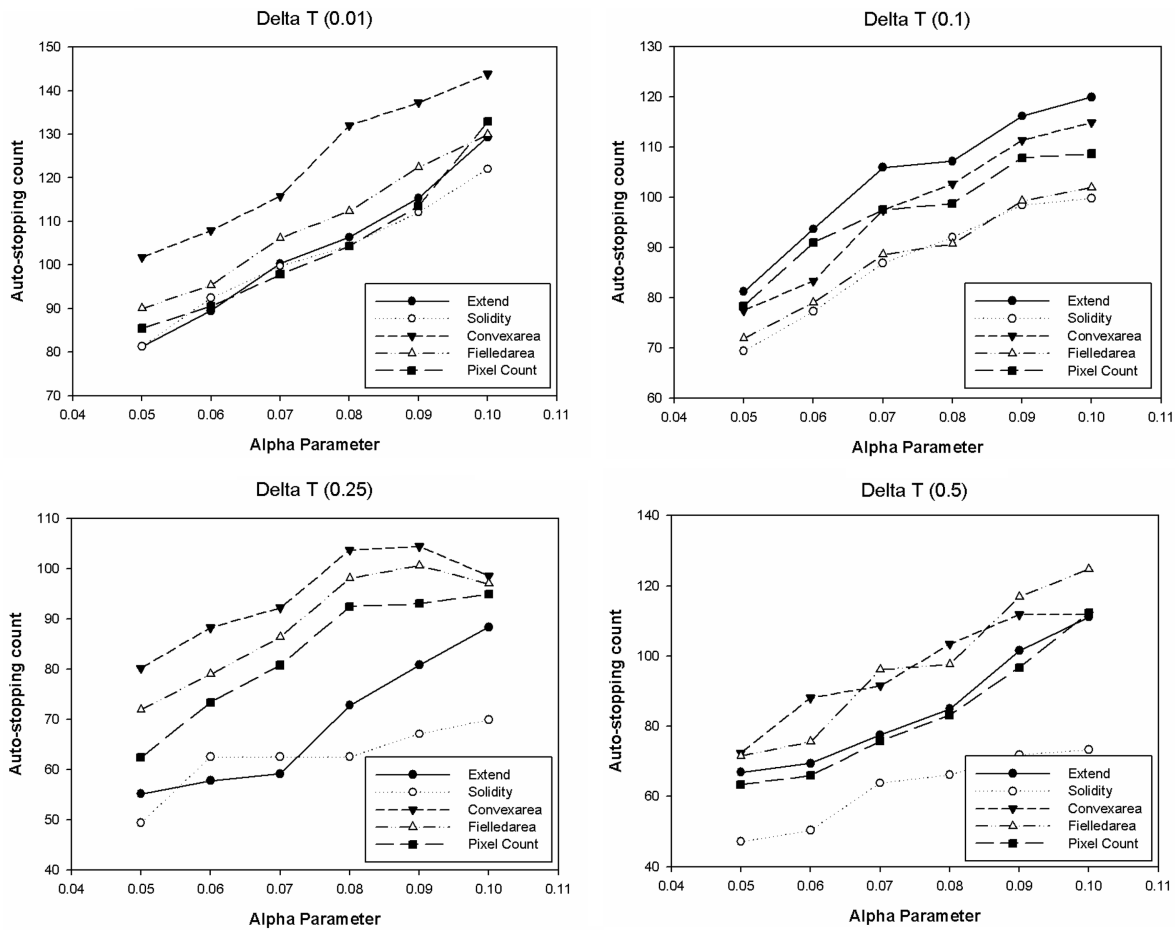

Fig. 7. Results show the mean value of stopping count for each FMI and α value of MTTT: (a) use Δt = 0.01 (b) use Δt = 0.1 (c) use Δt = 0.25 (d) use Δt = 0.5

AOR [31], as shown in Eq. (12), represents the degree of matching between the auto segment method and the manual method. And SCV, as shown in Eq. (13), is the indicator which simultaneously considers and represents accuracy and a minimum iteration count of image segmentation.

$$\text{AOR} = \frac{\text{Area (Auto} \cap \text{Manual)}}{\text{Area (Auto} \cap \text{Manual)}} \times 100\ \% \tag{12}$$

$$\text{SCV} = \frac{\text{AOR}}{\text{Iteration count}} \times 100 \tag{13}$$

3. Results

It is necessary to calculate the optimal Δt to guarantee the stability of the numerical iteration of the variational level set. Therefore, the value of Δt which satisfied the conditions of Eq. (5) about the ERC image was automatically calculated, Δt was calculated as 0.25 (Table 1). Excellent FMI was judged for the following result and the other result about Δt was compared and analyzed. If there is no optimal automatic stop function, iteration has a very difficult problem where it should stop. Therefore, the method suggested in this study is necessary.

We got the result of the automatic stop count calculated when MTTT was applied to each Δt of 0.01, 0.1, 0.25, and 0.5 and FMI candidates in this study. The mean value of each result was shown in Fig. 7(a) to (d).

In the results, we find the mean values of the automatic stop iteration count increased as the α values increased in all the FMIs except SI. The deviation values increased in all the FMIs, and SI was increased from 61.55 to 72.23 and CaI was done from 71.67 to 77.93. Finally, the above results have judged that the mean values of the automatic stop count and the deviation of SI (49.31 ± 57.31 in Δt 0.25 and 0.05) are excellent when the iterative calculation numbers were just considered because they were lowest in each delta T. Each mean shape model about myocardial images were made and used by making reference and accuracy of the suggested segmentation technique was verified. We can know the effectiveness of the segmentation method suggested through the evaluation of AOR

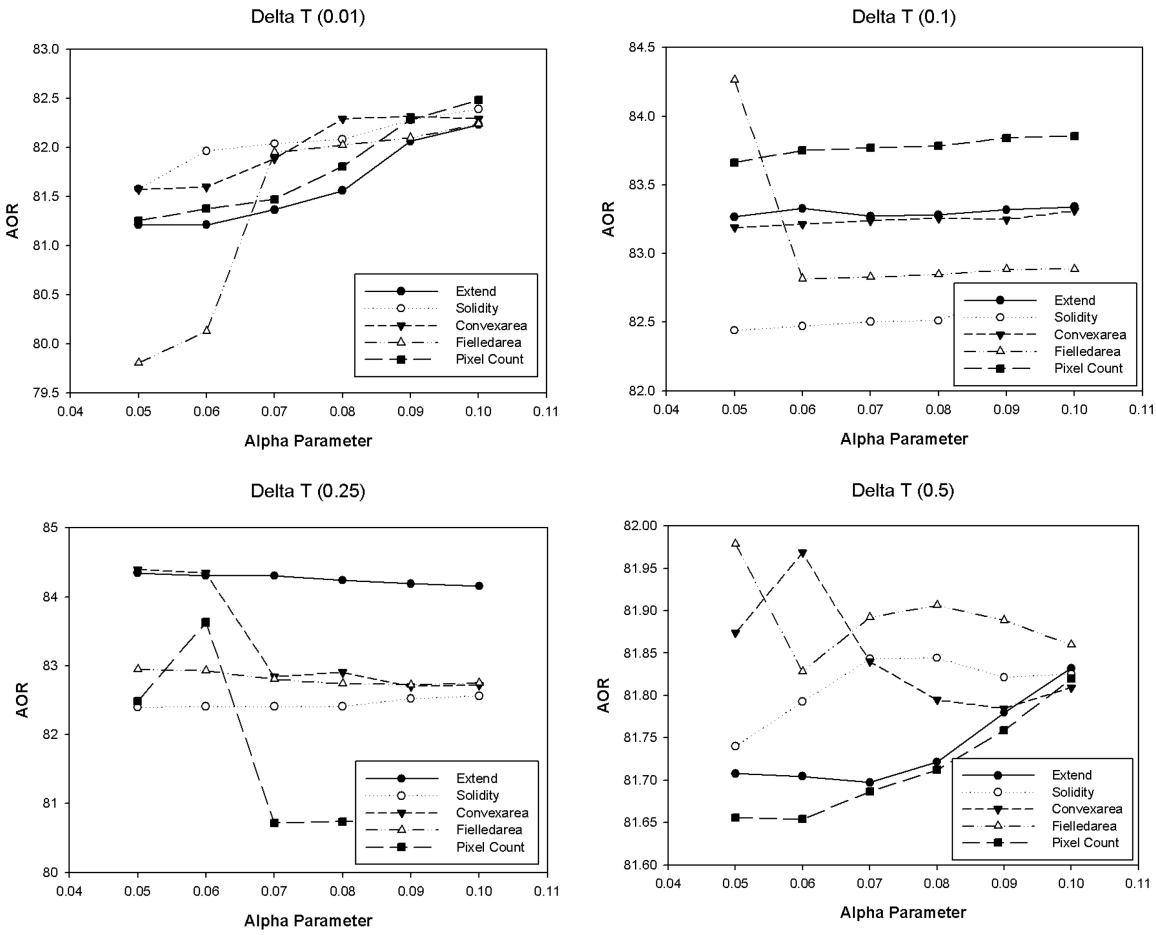

Fig. 8. Results show the mean value of AOR for each FMI and α value of MTTT: (a) use Δt = 0.01 (b) use Δt = 0.1 (c) use Δt = 0.25 (d) use Δt = 0.5

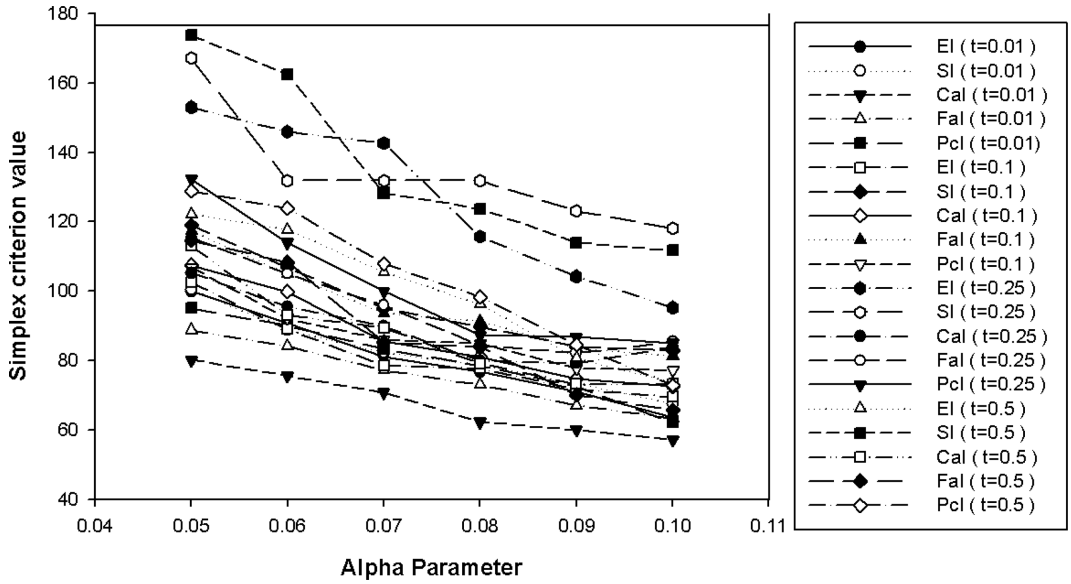

Fig. 9. Results show the mean value of SCV for each FMI and α value of MTTT: (a) use Δt = 0.01 (b) use Δt = 0.1 (c) use Δt = 0.25 (d) use Δt = 0.5

Table 2. Proposed segmentation auto stopping count and AOR results for MPS images.
(Delta T= 0.25, α=0.05, FMI=SI)

	Data set 1		Data set 2	
Slice No.	Auto stopping count (Iteration)	AOR (%)	Auto stopping count (Iteration)	AOR (%)
Slice 1	2	82.1	51	86.49
Slice 2	22	81.74	16	92.74
Slice 3	5	90.37	33	90.26
Slice 4	5	90.30	19	89.26
Slice 5	15	80.32	5	86.36
Slice 6	55	86.33	86	90.11
Slice 7	16	85.34	46	95.84
Slice 8	6	82.98	29	92.45
Slice 9	81	78.81	54	80.34
Slice10	33	95.90	38	97.58
Slice11	60	86.28	25	86.13
Slice12	55	83.05	75	86.12
Slice13	2	81.08	10	82.36
Slice14	60	84.11	27	80.18

and SCV. We can know excellent FMI in the FMI candidates and compare the results according to the CFL condition.

The result of AOR is shown when in Fig. 8. The deviation of CaI was increased from 10.49 to 10.64 and one of EaI was done from 10.53 to 10.72 as the α values increase.

In Fig. 9, we found that SI (delta T = 0.25, α = 0.05) were excellent, we can see the indicators that minimum automatic stop iteration count and AOR were simultaneously considered. The SCV values were reduced as the values increased and SI (delta T = 0.25) of them comparatively showed its stable pattern. Using the procedure presented above, we showed the representative case of test set images. We get a superior FMI and candidate FMI for exact auto segmentation from AOR comparison, to show the performance of the superior FMI (SI) to test set images, it was compared the auto stopping count and AOR (Table 2). The iteration count for segmentations depends on object shape complexity. In test set B case, the maximum count was 81 (slice 9), the minimum iteration count was 2 (slice 16), in the normal, case the maximum count was 86 (slice 6), the minimum iteration count was 5 (slice 5). Maximum AOR appeared in slice 10 (95.90 %); mean AOR was 83.24 % for all images and in test set 1 case. Maximum AOR appeared in slice 8 (95.84 %); the mean AOR was 86.87 % for all images.

From all experiments, the use of SI, delta 0.25 and alpha 0.05 was found to be the most accurate with decreasing iterations. We suggested a new segmentation method for the quantitative analysis of the myocardial. from the result, we can make a 3D myocardial model (Fig. 10) and quantitative analysis is possible

4. Discussions

We set three process steps for optimal segmentation in this study: 1) settling the stability problem. 2) manually assigning a heuristic iteration count to obtain myocardial

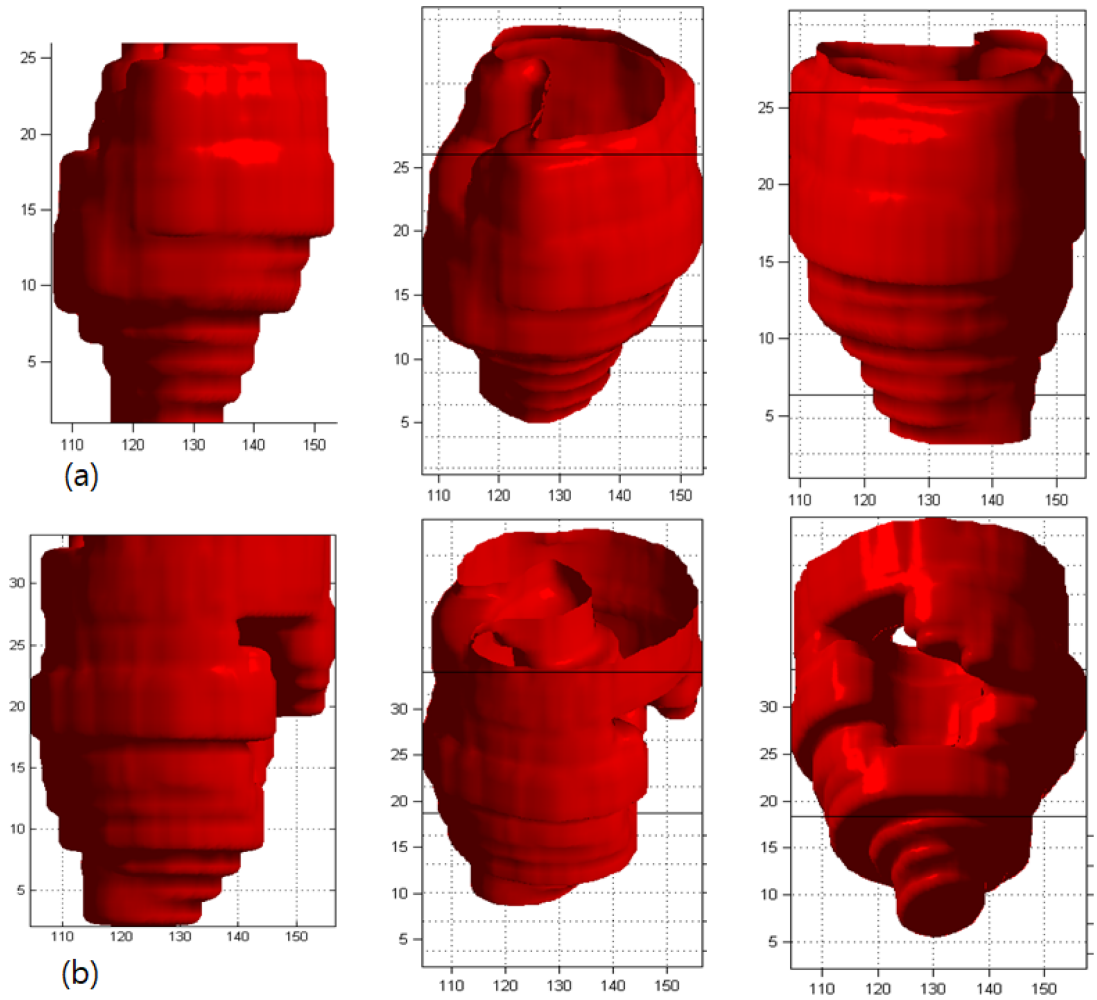

Fig. 10. (Color online) Left ventricle 3D model using the suggested segmentation method: (a) test case A, see from top to bottom, inner wall and outer wall simultaneously, (b) test case B, 3D myocardial model that shows defects; we can see a hole in the model.

features. 3) calculating the iteration stop count automatically from the FMI and modified Thompson Tau technique (MTTT). According to this procedure, we simulate myocardial segmentation. ERC images including normal and abnormal ones were used to take the test to find best FMI. The following method was used to evaluation the suggested segmentation method.

Manual segmentation of one image was repeatedly carried out 14 times by two experts and reference was made by a mean shape model. Manual segmentation of 292 times was conducted with a total of 28 images. In addition, in this study, how the automatic segmentation method suggested accord with reference was evaluated through the area overlap ratio (AOR) and the simplex criterion value (SCV). From all experiments, the use of SI, delta 0.1 and alpha 0.05 was found to be the most accurate with decreasing iterations.

We needed to solve the curve evolution for optimal stopping criteria. Almost all level set curve evolution has a predetermined iteration count value where the result can arrive at a local minimum [19]. In addition, the speed function of the level set must force the embedded curve to slow down and achieve a steady-state [16], but the speed function cannot force the curve evolution to reach a steady-state as a result of the iteration process.

The issue in this study is that it does not use an arbitrarily fixed iteration count to prevent early stopping or an excessive count. Using of this type of count will reduce the more calculation time and increase the accuracy of segmentation than the original CV model that the automatic stop technique was not applied.

The contents of the segmented results according to an iterative calculation by the step to segment images are shown in Fig. 2. If the iterative calculation numbers are insufficient, under-segmentation is done. If the iterative calculation numbers increase, over-segmentation is done

and the calculation time increases.

Stability is the approximation errors at each iteration that we encounter when a differential equation is numerically solved. SCV is used when the degree of stability of numerical iterations is estimated. Therefore, it can be found that excellent result drawn from $\Delta t = 0.25$ by calculating it through the CLF conditions contribute to stability.

FMI measurement distribution of myocardial obtained using the optimal Δt showed faster convergence and was more stable to the iteration than that when an arbitrarily assigned Δt was used, for example, when $\Delta t = 0.25$. Each FMI showed different results that could be used to settle the stopping problem in each FMI measurement result. The Tau factor means a small change in groups of FMI measurement distribution, and the first count from the Tau factor section is selected to auto-stop the iteration. However, if we change the α value, then the Tau factor sector is changed.

In this study, the 3D myocardial model enables us to see ischemic and infarction regions easily more than 2D images and also quantitative analysis is possible. So we can see the defect region, the inner wall and the outer wall are displayed simultaneously. We plan to compare and verify the accuracy with other methods to carry out the clinical case tests in the next study.

5. Conclusion

This paper presents a segmentation and a 3D myocardial model of the ERC images by the optimized level set method. The important point of the level set is when stopping iteration in order to obtain the optimal segmentation result. If we use the suggested optimized segmentation method, the question of when stopping iteration in order to obtain the optimal segmentation result can be solved. Additionally, the quantification of myocardial perfusion defects can be calculated from the 3D model based on this technology.

References

[1] K. S. Won and H. W. Kim, Nucl. Med. Mol. Imaging **43**, 196 (2009).
[2] A. K. Paul and H. A. Nabi, J. Nucl. Med. Technol. **32**, 179 (2004).
[3] J. G. Schwartz, R. B. Johnson, F. C. Aepfelbacher, J. A. Parker, L. Chen, R. R. Azar, R. A. Parker, and P. G. Danias, Nucl. Med. Commun. **24**, 543 (2003).
[4] D. Knollmann, O. H. Winz, P. T. Meyer, M. Raptis, T. Krohn, K. C. Koch, and W. M. Schaefer, J. Nucl. Med. **49**, 1636 (2008).
[5] K. Zsolt, B. Laszlo, G. Laszlo, V. Jozsef, H. Ida, F. Tibor, B. Emilia, J. Csaba, S. Gabor, K. Rudolf, R. Ildiko, and E. Istvan, Comput. Med. Imaging Graph. **31**, 577 (2007).
[6] L. Dornheim, K. D. Tönnies, and J. Dornheim, Proc. MICCAI 335 (2005).
[7] R. Yang, M. Mirmehdi, and D. Hall, Proc. MICCAI 171 (2006).
[8] W. H. Tan and R. Besar, LNCS 5857, 38 (2009).
[9] D. Éric, B. Michel, A. Gilles, L. Ivan, and D. Jacques, IEEE Trans. Med. Imaging **20**, 643 (2001).
[10] T. Kohlberger, G. Funka-Lea, and V. Desh, LNCS 4791, 327 (2007).
[11] T. Chan and L. Vese, IEEE Trans. Imag Proc. **10**, 266 (2001).
[12] R. Malladi, J. A. Sethian, and B. C. Vemuri, IEEE Trans. Patt. Anal. Mach. Intell. **17**, 158 (1995).
[13] S. Osher and J. A. Sethian, J. Comp. Phys. **79**, 12 (1998).
[14] J. A. Sethian, Cambridge University Press (1999).
[15] S. Choi, H. C. Kim, J. Oh, T. Kang, K. Sun, and M. Kim, IEEE NSS/MIC 3060-4 (2007).
[16] K. Chaudhury and K. R. Ramakrishnan, Patt. Recg. Letters **28**, 884 (2007).
[17] A. Mansouri and J. Konnard, IEEE Trans. PAMI 24 201-9 (2002).
[18] A. Mansouri, IEEE Trans. PAMI **24**, 947 (2002).
[19] Y. Jung, K. T. Chu, and S. Torquato, J. Comp. Phys. **223**, 711 (2007).
[20] Michele R Find Outliers with Thompson Tau. Available at : http://www.mathworks.com/matlabcentral/fileexchange/authors/95943
[21] R. Thompson, Journal of the Royal Statistical Society **47**, 53 (1985).
[22] L. Vincent and P. Soille, IEEE Trans. PAMI **13**, 583 (1991).
[23] M. Bhagwat and R. K. Krishna, Pise VE 2010 Simplified watershed transformation IJCSC **1**, 175 (2010).
[24] M. Debakla, K. Djemal, and M. Benyettou, Journal of Applied Sciences **4**, 101 (2011).
[25] Z. Huiyu, S. Gerald, and S. Chunmei, Studies in Fuzziness and Soft Computing **242**, 257 (2009).
[26] L. A. Guner, N. I. Karabacak, T. Cakir, O. U. Akdemir, S. A. Kocaman, A. Cengel and M. Unlu, Eur. J. Nucl. Med. Mol. Imaging **37**, 2070 (2010).
[27] A. Wolak, P. J. Slomka, M. B. Fish, S. Lorenzo, W. Acampa, D. S. Berman, and G. Germano, J. Nucl. Cardiol. **15**, 27 (2008).
[28] Milan Lomsky, Clin. Physio.l Funct. Imaging **25**, 234 (2005).
[29] T. F. Cootes, C. J. Taylor, D. H. Cooper, and J. Graham, Comput. Vis. Image. Understand **61**, 38 (1995).
[30] S. Choi and C. Kim, Healthc. Inform Res. **16**, 36 (2010).
[31] Y. Yuan, M. L. Giger, H. Li, K. Suzuki, and C. Sennett, Med. Phys. **34**, 4180 (2007).
[32] H. Jadvar, H. W. Strauss, and G. M. Segall, SPECT and PET in the evaluation of coronary artery disease Radio-

graphics **19**, 915 (1999).
[33] T. L. Faber, C. D. Cooke, R. D. Folks, J. P. Vansant, K. J. Nichols, E. G. DePuey, R. I. Pettigrew, and E. V. Garcia, J. Nucl. Med. **40**, 659 (1999).
[34] L'Annunziata, Michael F. (2007). Radioactivity: introduction and history, Elsevier BV. ISBN 978-0-444-52715-8, Amsterdam, Netherlands (2007) pp 55-58.
[35] W. R. Hendee and E. R. Ritenour, Medical Imaging Physics, Fourth Edition Wiley-Liss Inc (2002)
[36] C. M. Gomes, A. J. Abrunhosa, P. Ramos, and E. K. J. Pauwels, Advanced Drug Delivery Reviews **63**, 547 (2011).
[37] The MathWorks,Inc. image processing toolbox, https://kr.mathworks.com/